

Orbital-Selective Spin-Triplet Superconductivity in Infinite-Layer LaNiO_2

Fabian Jakubczyk,^{1,2,*} Armando Consiglio,^{2,3,4} Domenico Di Sante,⁵ Ronny Thomale,^{2,3} and Carsten Timm^{1,2}

¹*Institute of Theoretical Physics, Technische Universität Dresden, 01069 Dresden, Germany*

²*Würzburg-Dresden Cluster of Excellence ct.qmat, Germany*

³*Institut für Theoretische Physik und Astrophysik,
Universität Würzburg, 97074 Würzburg, Germany*

⁴*Istituto Officina dei Materiali, Consiglio Nazionale delle Ricerche, Trieste I-34149, Italy*

⁵*Department of Physics and Astronomy, University of Bologna, 40127 Bologna, Italy*

(Dated: December 4, 2024)

The discovery of superconductivity in infinite-layer nickelates has ignited stark interest within the scientific community, particularly regarding its likely unconventional origin. Conflicting magnetotransport measurements report either isotropic or anisotropic suppression of superconductivity in an external magnetic field, with distinct implications for the nature of superconducting order. In order to ensure a most suited model subject to subsequent many-body analysis, we develop a first-principles-guided minimal theory including Ni $d_{x^2-y^2}$, La $d_{3z^2-r^2}$, and La d_{xy} orbitals. Amended by the consideration of orbital-selective pairing formation, which emphasises the correlation state of the Ni $3d_{x^2-y^2}$ orbital, we calculate the superconducting ordering susceptibility mediated by spin fluctuations. We find a parametric competition between even-parity d -wave and, in contrast to previous studies, odd-parity p -wave pairing, which becomes favorable through a large quasiparticle weight renormalization for Ni $3d_{x^2-y^2}$ electrons. Our findings not only shed light on the distinctiveness of LaNiO_2 as compared to cuprate superconductors or nickelates of different rare-earth composition but also suggest similarities to other candidate odd-parity superconductors.

Introduction.—Since the initial discovery of superconductivity in Sr-doped NdNiO_2 thin films [1], the family of nickelate superconductors has kept on growing and by now also includes $\text{La}_{1-x}\text{Sr}_x\text{NiO}_2$, $\text{Pr}_{1-x}\text{Sr}_x\text{NiO}_2$, and $\text{La}_{1-x}\text{Ca}_x\text{NiO}_2$ [2, 3]. Most intriguingly, some groups report the onset of superconductivity even in undoped infinite-layer (IL) nickelates, suggesting that the eventual ground state of sufficiently clean parent nickelates is a superconducting (SC) state [2, 4–7]. Despite being isostructural to high T_c cuprates, the extend of similarity between these materials remains partially unclear, in spite of numerous studies addressing this issue [8–12].

A fundamental subject of discussion is the symmetry of the SC order parameter (OP). On the one hand, magnetotransport measurements indicate isotropic Pauli-limited behavior with singlet pairing and even parity in the IL nickelate $\text{Nd}_{0.775}\text{Sr}_{0.225}\text{NiO}_2$ [13]. This scenario was supported by many theoretical investigations, mostly pointing at d -wave order like in the cuprates [14–19]. On the other hand, evidence for anisotropic superconductivity that violates Pauli limiting and potential spin-triplet pairing was reported in La-based nickelate thin films [5, 20, 21]. Likewise, this anisotropic limiting behavior for different magnetic-field orientations has recently been observed for free-standing IL nickelate membranes [22]. Variations in the upper critical field within the nickelate family were ascribed to the different rare-earth (RE) elements, i.e., the magnetic character of the $4f$ electrons for the Nd^{3+} Kramers doublet as opposed to their absence in La^{3+} , or the nonmagnetic singlet ground state of Pr^{3+} [23].

In this Letter, we address the open question of gap structure and potential odd-parity pairing in IL LaNiO_2 .

The largest deviation from the cuprates as well as the strongest effective-mass enhancement can be expected in the absence of doping. A direct comparison between for instance NdNiO_2 and LaNiO_2 reveals that this effect is particularly strong in the lanthanum compound [16]. Moreover, LaNiO_2 does not host any $4f$ electrons, who may influence the SC pairing [24]. Hybridization with $4f$ electrons is expected to be non-negligible in Nd and Pr nickelates [24–27]. To resolve this puzzle, we adopt the perspective of spin-fluctuation-mediated unconventional superconductivity [28] and incorporate the effect of increased correlations via the orbital-selective approach known from iron-based superconductors [29, 30]. Our calculations reveal that spin-triplet pairing can indeed be realized in LaNiO_2 , once an enhanced effective mass of the Ni $3d_{x^2-y^2}$ electrons is taken into account.

Low-energy electronic structure.—In contrast to the parent compounds of the cuprates, which exhibit long-range antiferromagnetic order, clear signatures of long-range magnetism are lacking for IL nickelates, suggesting a paramagnetic ground state, in particular for LaNiO_2 [31–33]. Magnetism is often triggered by strong electronic correlations, which indeed exist in IL nickelates [9, 16, 34, 35]. In fact, stable magnetic order was proposed based on *ab-initio* calculations [9, 25, 36, 37]. The unexpected absence of long-range magnetic order might be explained by the coupling to itinerant RE electrons, i.e., by the destruction of long-range order via self-doped holes, an effect not well captured by mean-field calculations [9, 38]. Nevertheless, nonlocal spin fluctuations have been observed in IL nickelates [14–16, 25, 32, 33, 38–40], which makes spin-fluctuation-mediated superconductivity the most reasonable mechanism. Furthermore,

muon spin rotation (μ SR) has recently demonstrated intrinsic short-range magnetic order, also in the superconducting state [4]. Scanning-SQUID measurements found paramagnetic response in $\text{La}_{0.85}\text{Sr}_{0.15}\text{NiO}_2$, together with an inhomogeneous ferromagnetic background independent of the RE element [41]. However, short-range magnetic order is not expected to significantly alter the electronic band structure since magnetic effects lacking long-range periodicity are averaged out. This results in a Fermi surface that is very similar to the one in the absence of magnetism. The excellent match between recent ARPES measurements on Sr-doped LaNiO_2 [42] and band-structure calculations of non-magnetic LaNiO_2 [12, 14, 35, 37, 42] supports this conclusion.

In non-magnetic LaNiO_2 , the principal contribution at the Fermi level arises from a band primarily governed by Ni $3d_{x^2-y^2}$ electrons. This results in a large hole-like and mostly two-dimensional (2D) Fermi surface (FS) similar to the cuprates. In addition, another hybridized band of mixed Ni $3d$ and La $5d$ character creates small ellipsoidal, electron-like pockets around the Γ and A high-symmetry points of the Brillouin zone, indicating the multiorbital and three-dimensional (3D) character of LaNiO_2 [12, 37, 43]. These two electron pockets enable self-hole-doping of the large $d_{x^2-y^2}$ Fermi sheet, a process with major involvement of La $5d$ states [9, 34]. Especially La $5d_{z^2}$ and La $5d_{xy}$ orbitals are known to have significant weight on the FS [9, 12, 14], where d_{z^2} is a shorthand notation for $d_{3z^2-r^2}$. Furthermore, these partially occupied electron pockets might give rise to the negative Hall coefficient, to the slightly metallic behavior of the resistivity at high temperatures, and possibly even to the superconductivity in undoped IL nickelates [2, 3, 14].

Hole-doping the system for instance with Sr induces changes in the electronic structure. It reduces the self-doping effect by first shifting the Γ pocket above E_F , followed by the pocket around A in the overdoped region [9, 16, 42, 44, 45]. Furthermore, doping reduces the charge-transfer energy [44], i.e., overall increases the cuprate-like character of the nickelates. However, the impact on LaNiO_2 is expected to be less pronounced compared to Nd-/Pr-based compounds regarding charge carriers, which is evidenced by the persistent negative Hall coefficient of $\text{La}_{1-x}\text{Sr}_x\text{NiO}_2$ even upon doping [2, 3].

In our effective low-energy Hamiltonian, based on the non-magnetic electronic structure of the system, we thus include Ni $d_{x^2-y^2}$, La d_{z^2} , and La d_{xy} orbitals and introduce the operator $\psi_\sigma^\dagger(\mathbf{k}) = [c_{1\sigma}^\dagger(\mathbf{k}), c_{2\sigma}^\dagger(\mathbf{k}), c_{3\sigma}^\dagger(\mathbf{k})]$ to describe the given multiband system. Here, $c_{l\sigma}^\dagger(\mathbf{k})$ is the fermionic creation operator, where σ and l denote the spin and orbital index, with $l = 1, 2, 3$ referring to the La $5d_{z^2}$, La $5d_{xy}$, and Ni $3d_{x^2-y^2}$ orbital, respectively. We thus write the non-interacting Hamiltonian as

$$H_0 = \sum_{\mathbf{k}\sigma} \psi_\sigma^\dagger(\mathbf{k}) h(\mathbf{k}) \psi_\sigma(\mathbf{k}), \quad (1)$$

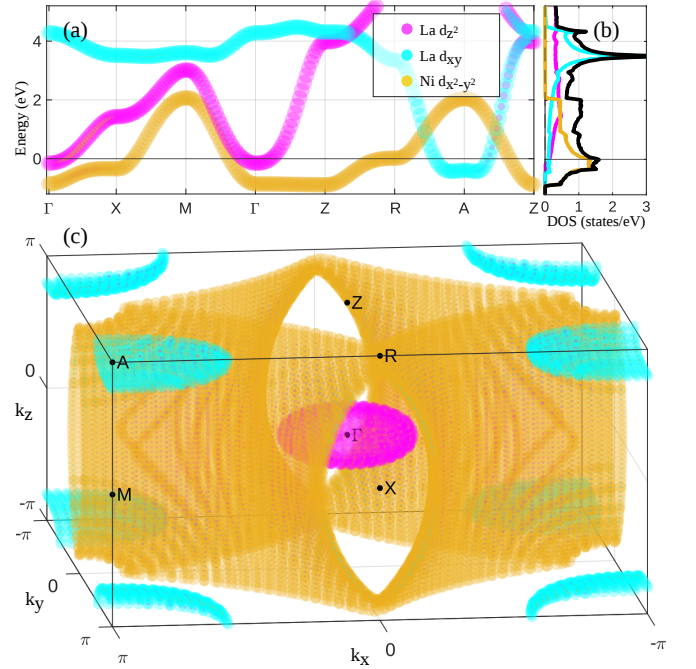


FIG. 1. (a) Band structure, (b) density of states, and (c) 3D Fermi surface including the orbital contributions relevant for the low-energy description of pristine LaNiO_2 . Magenta, cyan, and yellow refer to the La d_{z^2} , La d_{xy} , and Ni $d_{x^2-y^2}$ orbitals, respectively.

where $h(\mathbf{k})$ is constructed utilizing hopping amplitudes obtained from the Wannier downfolding of the band structure derived from density functional theory (DFT), wherein spin polarization is not taken into account. Thereby, we capture the important characteristics, as well as the distribution of orbital characters, of the non-magnetic FS in agreement with previous DFT [14, 25, 46] and alternative approaches such as DFT+ U [9, 47], DFT + dynamical mean-field theory (DMFT) [35, 37] or the GW approximation [48]. Details on the *ab-initio* calculations including further justification of the non-magnetic electronic structure, as well as the Hamiltonian $h(\mathbf{k})$ are given in the Supplemental Material (SM) [49]. In Fig. 1, we plot the orbitally resolved single-particle band structure, as well as the corresponding 3D FS and density of states (DOS) of our minimal model. Here, La $5d_{z^2}$ weight is located mostly around Γ , while the La $5d_{xy}$ electrons have a major contribution around the A point.

Strong correlations and magnetic response.—Orbitally differentiated correlations play an important role in IL nickelates. In particular the Ni $3d_{x^2-y^2}$ electrons are highly correlated, suggesting that they are in the vicinity of a Mott critical regime [37]. This is evidenced by an enhanced effective mass and thus reduced quasiparticle weight Z , which is significantly smaller for the Ni $d_{x^2-y^2}$ orbital compared to the other $3d$ orbitals [16, 18, 35]. In our work, we therefore focus on the effect of a highly correlated Ni $d_{x^2-y^2}$ orbital. Previous studies have re-

ported specific values of either the effective mass or the renormalization factor Z ($m^*/m = 1/Z$) in LaNiO_2 , ranging from $m^*/m \approx 2.81$ ($Z_{d_{x^2-y^2}} \approx 0.35$) [35, 37], over $m^*/m \approx 4.1$ ($Z_{d_{x^2-y^2}} \approx 0.24$) [50] to $m^*/m \approx 5.5$ ($Z_{d_{x^2-y^2}} \approx 0.18$) [16] and $m^*/m \approx 7$ ($Z_{d_{x^2-y^2}} \approx 0.14$) [51] or even lower ($Z_{d_{x^2-y^2}} \approx 0$) [18]. Doping would shift the Ni $d_{x^2-y^2}$ orbital away from half filling, where electronic correlations are strongest, leading to a reduced mass enhancement [16, 18, 37, 50].

We take this correlation-induced renormalization into account by means of the orbital selective ansatz [29, 30]. In this ansatz, quasiparticles in orbital l are weighted by a factor $\sqrt{Z_l}$, i.e., $c_l^\dagger(\mathbf{k}) \rightarrow \sqrt{Z_l}c_l^\dagger(\mathbf{k})$ and the Green's function in the orbital basis becomes

$$\tilde{G}_{ll'}(\mathbf{k}, \omega_n) = \sqrt{Z_l Z_{l'}} \sum_{\mu} \frac{a_{\mu}^l(\mathbf{k}) a_{\mu}^{l'*}(\mathbf{k})}{i\omega_n - E_{\mu}(\mathbf{k})}, \quad (2)$$

where $E_{\mu}(\mathbf{k})$ is the eigenenergy of band μ . Subsequently, the bare susceptibility in orbital space $\chi_{l_1 l_2 l_3 l_4}^0$ requires a straightforward multiplication by the quasiparticle weights to derive the corresponding quantity

$$\tilde{\chi}_{l_1 l_2 l_3 l_4}^0(\mathbf{q}, \omega) = \sqrt{Z_{l_1} Z_{l_2} Z_{l_3} Z_{l_4}} \chi_{l_1 l_2 l_3 l_4}^0(\mathbf{q}, \omega) \quad (3)$$

in the correlated system [29, 30, 39].

In the next step, we introduce local electron-electron interactions via a multiorbital Hubbard-Hund Hamiltonian

$$\begin{aligned} H_{\text{int}} = & U_{\text{Ni}} \sum_i n_{i\uparrow} n_{i\downarrow} \\ & + U_{\text{La}} \sum_i n_{il\uparrow} n_{il\downarrow} + U'_{\text{La}} \sum_{i,l',l} n_{il} n_{il'} \\ & + J_{\text{La}} \sum_{i,l',l} \sum_{\sigma\sigma'} c_{il\sigma}^\dagger c_{il'\sigma'}^\dagger c_{il'\sigma} c_{il\sigma} \\ & + J'_{\text{La}} \sum_{i,l',l} c_{il\uparrow}^\dagger c_{il'\downarrow}^\dagger c_{il'\downarrow} c_{il\uparrow}, \end{aligned} \quad (4)$$

where the coupling constants U , U' , J , and J' denote the intraorbital Coulomb, interorbital Coulomb, Hund's, and pair-hopping interactions, respectively. The orbital indices $l, l' \in (1, 2)$ run over the La $5d$ orbitals d_{z^2} and d_{xy} . Throughout our calculations, we apply the relations $U' = U - (J + J')$ and $J' = J$ between the coupling constants, which are satisfied in various orbital degenerate models and if orbital wave functions can be chosen real [52, 53]. Guided by prior research [14, 18, 35, 37, 50, 54], we estimate the interaction strengths in this material by $U_{\text{La}}/U_{\text{Ni}} = 0.5$ and consider the values $J_{\text{La}}/U_{\text{La}} = 0.2$, as well as $J'_{\text{La}}/U_{\text{La}} = 0.1$. The inclusion of on-site Hund's coupling J , i.e., of intra-atomic exchange interactions is expected to be an important ingredient for capturing the correlation physics. LaNiO_2 shows characteristic Hund's metal signatures such as the unexpected absence of long-range magnetism, the importance of high-spin

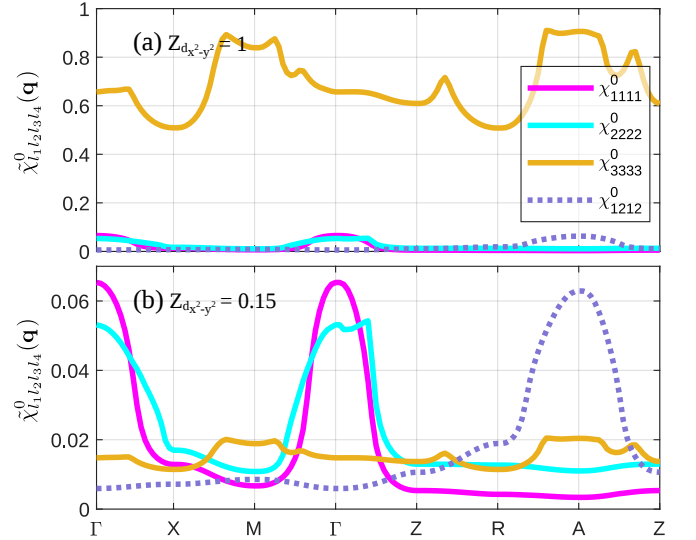


FIG. 2. Static bare susceptibilities $\tilde{\chi}_{l_1 l_2 l_3 l_4}^0(\mathbf{q}, \omega = 0)$ of parent LaNiO_2 for (a) $Z_{d_{x^2-y^2}} = 1$ and (b) $Z_{d_{x^2-y^2}} = 0.15$. Magenta, cyan, and yellow refer to the pure La d_{z^2} , La d_{xy} and Ni $d_{x^2-y^2}$ orbital contributions, respectively. The interorbital bare susceptibility $\tilde{\chi}_{1212}^0$ is shown in purple. We use $80 \times 80 \times 80$ \mathbf{k} -points for momentum space integration.

configurations, metallicity, orbital differentiation, and a decrease of $Z_{d_{x^2-y^2}}$ with stronger Hund's coupling J [18, 35, 37, 54]. These interactions are included in the calculation of susceptibilities within the random phase approximation (RPA). Note that in RPA the spin susceptibility systematically diverges once the interaction exceeds a critical value U_c and indicates a spin-density-wave instability, below which superconductivity emerges induced by spin fluctuations.

In Figs. 2(a) and 2(b), the non-interacting susceptibilities $\tilde{\chi}_{l_1 l_2 l_3 l_4}^0(\mathbf{q}, 0)$ are shown separately for the orbital contributions $l = 1, 2, 3$ referring to La $5d_{z^2}$, La $5d_{xy}$, and Ni $3d_{x^2-y^2}$, respectively. Figure 2(a) addresses the unrenormalized case, with the main peaks located around the M and A points, similar to the cuprates [55]. These magnetic fluctuations are dominated by Ni $d_{x^2-y^2}$ electrons and strongly enhanced upon introducing interactions at the RPA level. In contrast, the diagonal contributions of the La d_{z^2} and d_{xy} orbital reach their maximum around Γ . Moreover, we observe a sizable interorbital $\tilde{\chi}_{1212}^0$ feature around the A point.

Sufficient reduction of the Ni $d_{x^2-y^2}$ quasiparticle weight results in a clear dominance of fluctuations stemming from the RE orbitals, as can be seen in Fig. 2(b), where $Z_{d_{x^2-y^2}} = 0.15$. Interactions predominantly lead to an enhancement of the diagonal La $5d$ peaks around Γ but also of interorbital $\tilde{\chi}_{1122}^{\text{RPA},s}$ and $\tilde{\chi}_{1221}^{\text{RPA},s}$ contributions around Γ and A, respectively. The latter are not notable on the bare level but in particular the $\tilde{\chi}_{1122}^{\text{RPA},s}$ component diverges together with the intraorbital spin susceptibilities $\tilde{\chi}_{1111}^{\text{RPA},s}$ and $\tilde{\chi}_{2222}^{\text{RPA},s}$ upon approaching U_c .

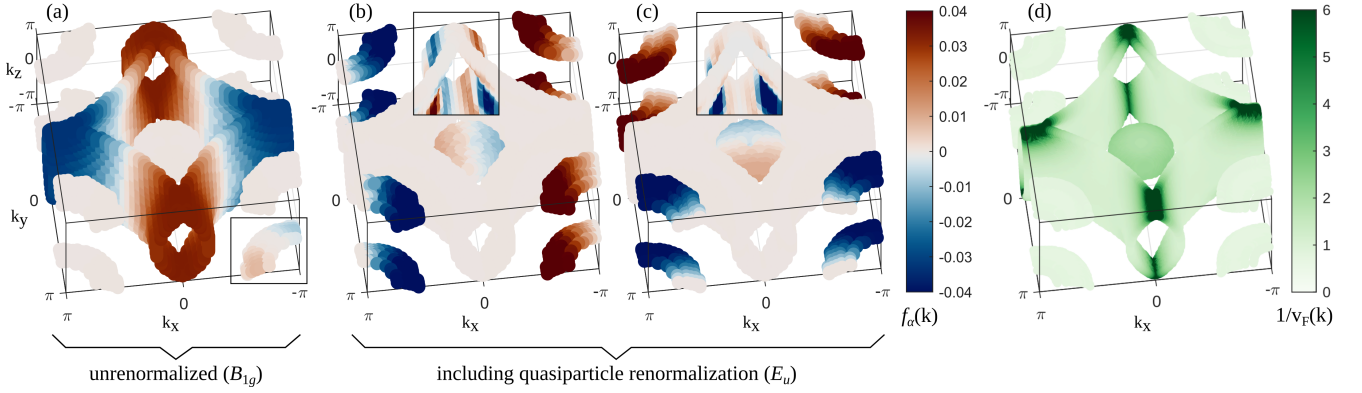


FIG. 3. Leading pairing structure of LaNiO₂ (a) without and (b), (c) with inclusion of quasiparticle renormalization. The gap symmetry changes from (a) an even-parity d -wave to (b), (c) a degenerate odd-parity p -wave solution. A color scale highlighting smaller amplitudes with maximum value of $\pm 1 \times 10^{-4}$ was chosen for the insets to reveal, e.g., in panels (b), (c), the horizontal line nodes on the large FS. (d) Inverse Fermi-velocity $1/v_F(\mathbf{k}) = 1/|\nabla_{\mathbf{k}} E_\nu(\mathbf{k})|$ giving a measure of the DOS. A total of 8504 points is taken for the 3D gap-structure calculations and we use $60 \times 60 \times 60$ \mathbf{k} -points for momentum space integration.

Previous calculations of the LaNiO₂ static weak-coupling spin susceptibility for $\mathbf{q} = (q_x, q_y, 0)$ with converged DFT + DMFT Green's functions similarly resulted in a maximum near Γ [34]. Such a transition from primarily anti-ferromagnetic to ferromagnetic fluctuations stresses the necessity of reevaluating the SC pairing symmetries in the regime of strongly renormalized Ni $3d$ quasiparticle weights.

Spin-fluctuation pairing.—Magnetic fluctuations are seen as a strong candidate for mediating superconductivity in IL nickelates [14–16, 25, 32, 33, 38–40]. In order to compute the SC pairing interactions, we thus employ a formalism based on spin-fluctuations [56–58] with the adjustment of additional quasiparticle renormalization when projecting the pairing interaction from orbital to band space [30, 39]. For this purpose, we solve the linearized gap equation

$$\lambda_\alpha f_\alpha(\mathbf{k}) = \sum_j \oint_{C_j} \frac{d^2 k'_\parallel}{(2\pi)^2 v_F(\mathbf{k}')} \tilde{\Gamma}_{ij}(\mathbf{k}, \mathbf{k}') f_\alpha(\mathbf{k}'), \quad (5)$$

the eigenvalues of which determine the pairing strength λ_α for the various pairing channels α [59]. The largest eigenvalue results in the highest transition temperature [57], while its eigenfunction $f_\alpha(\mathbf{k})$ identifies the gap symmetry. $\tilde{\Gamma}_{ij}(\mathbf{k}, \mathbf{k}')$ represents the renormalized form of the effective multiorbital pair scattering vertex and momenta $\mathbf{k} \in C_i$, $\mathbf{k}' \in C_j$ are constrained to the FS sheets $C_{i,j}$. A momentum-dependent measure of the DOS is given by the inverse Fermi velocity $1/v_F(\mathbf{k}) = 1/|\nabla_{\mathbf{k}} E_\nu(\mathbf{k})|$, which is shown in Fig. 3(d) for the rigid bands of our model. Here, van Hove features can be observed on the hole-like FS near the R points. In order to convert the integral equation (5) to an algebraic matrix equation that can be solved numerically, the area of the discretized Fermi surface segments is determined using a Delaunay triangulation procedure [30, 60].

In Fig. 3, we present the leading gap-symmetry functions $f_\alpha(\mathbf{k})$ for (a) the unrenormalized and (b), (c) the renormalized scenario. Unsurprisingly, a simple d -wave singlet solution is clearly favored for $Z_l = 1$, i.e., when orbital-selective renormalization is disregarded. Such a state belongs to the B_{1g} irreducible representation of the point group D_{4h} , which describes the underlying tetragonal lattice. Here, Cooper pairing from the Ni $3d_{x^2-y^2}$ orbital is predominant, with an almost vanishing gap on the RE electron pockets around Γ and A. This cuprate-like SC order has been suggested previously based on spin fluctuations [14–17, 19, 39].

Once we shift our model into the strongly correlated regime of $Z_{d_{x^2-y^2}} \lesssim 0.2$, solving the linearized gap equation (5) yields drastically altered results. The SC gap is now largest on the La dominated pockets, since the Ni $d_{x^2-y^2}$ quasiparticle DOS is strongly reduced. Even more importantly, two degenerate p -wave functions be-

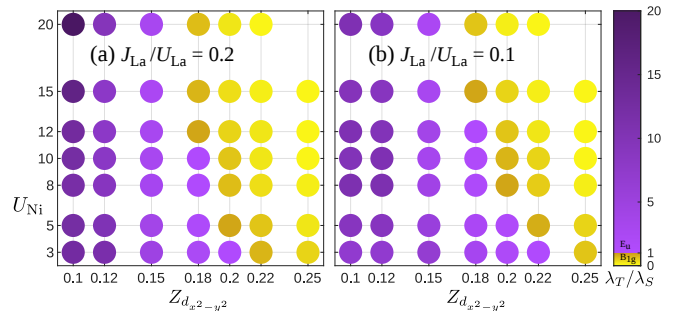


FIG. 4. Interaction- and renormalization-dependent leading solutions of the linearized gap equation for $U_{\text{La}}/U_{\text{Ni}} = 0.5$ and (a) $J_{\text{La}}/U_{\text{La}} = 0.2$, (b) $J_{\text{La}}/U_{\text{La}} = 0.1$. The color scale represents the ratio λ_T/λ_S of the eigenvalues of the favored triplet and singlet channel. The pairing symmetry is E_u or B_{1g} for a leading triplet or singlet state, respectively.

come favored, including a sign change on the large FS as a function of k_z and thus opposite signs on the pockets near Γ and A. These p -wave solutions belong to the two-dimensional representation E_u and are likely realized in the time-reversal-symmetry-breaking (TRSB) state, for which the weak-coupling condensation energy becomes largest compared to the remaining possible combinations of the p_x and p_y solution [61]. In the presence of weak spin-orbit coupling (see SM [49]), one naturally expects an alignment between the z -direction of the spin wave function and the crystalline c -axis [62]. Therefore, we can analytically approximate the numerically calculated SC OP of this spin-triplet state by

$$\mathbf{d}(\mathbf{k}) = \Delta_0 \hat{\mathbf{z}} \cos k_z (\sin k_x \pm i \sin k_y), \quad (6)$$

with the magnitude of the quasiparticle gap

$$\Delta_{\mathbf{k}} = |\mathbf{d}(\mathbf{k})| = \Delta_0 \sqrt{\cos^2 k_z (\sin^2 k_x + \sin^2 k_y)}. \quad (7)$$

Such a state is often referred to as chiral p -wave. Moreover, it is analogous to the so-called Anderson-Brinkman-Morel (ABM or axial) phase of ^3He [63, 64] and has been debated extensively, e.g., for Sr_2RuO_4 [61, 62, 65]. The gap resulting from the \mathbf{d} vector in (6) has point nodes on the electron pockets for $k_x, k_y = 0, \pm\pi$ and $k_z = \pm k_F$. In addition, line nodes are located on the large hole-like FS for $k_x, k_y = k_F$ and $k_z = \pm\pi/2$. In Fig. 4, we present RPA calculations over an extensive range of input parameters to substantiate the robustness of our results. Intriguingly, our conclusions even hold when the effect of doping is included as a rigid shift of the chemical potential such that the pocket around Γ vanishes (see SM [49]). However, a reduced mass enhancement due to doping might have a compensating effect. One potential yet unexplored scenario involves the doping-induced transition to a distinct OP within the SC dome.

Our proposal of chiral p -wave superconductivity with $\mathbf{d} \parallel \hat{\mathbf{z}}$ could explain the experimentally observed weaker suppression of superconductivity for an external magnetic field oriented within the basal plane [5, 20, 22, 23]. For triplet superconductors, one would generally not expect Pauli suppression if $\mathbf{d} \cdot \mathbf{H} = 0$, i.e., the alignment $\mathbf{d} \parallel \mathbf{H}$ maximizes paramagnetic limiting effects. Moreover, the gap in Eq. (7) has point nodes and thus could cause the quadratic temperature dependence of the London penetration depth [66, 67], which was attributed to a superconductor with line nodes in the presence of disorder [68, 69]. Small deviations from quadratic scaling may result from additional weight at the Fermi level, due to the horizontal line nodes on the Ni $d_{x^2-y^2}$ dominated FS with low quasiparticle DOS. Besides, recent μSR measurements provided evidence for the coexistence of short-range magnetic order and superconductivity in IL nickelates [4], which indicates TRSB.

Summary and conclusions.—Our calculations of magnetic fluctuations and the resulting pairing symmetries

reveal potential topological $p_x + ip_y$ superconductivity in IL LaNiO_2 , once an orbital-selective quasiparticle renormalization is introduced for the Ni $d_{x^2-y^2}$ electrons. From our results, we can conclude that RE physics in LaNiO_2 is not merely important for the explanation of a negative Hall conductivity [2] but that superconductivity could actually emerge from the associated bands. However, one should keep in mind that the RE metal representative strongly affects the observed phenomenology of IL nickelates. Additionally, the proposed p -wave order would resolve the controversy surrounding the anisotropic high-field limiting behavior obtained from magnetotransport measurements [5, 20, 22], as well as the quadratic temperature dependence of the penetration depth [66–69]. In this regard, our effective Hamiltonian captures the relevant physics for superconductivity in 112 lanthanum nickelates, highlighting the importance of multiorbital processes and the 3D fermiology.

To conclude, our comprehensive investigation provides strong evidence that IL LaNiO_2 could exhibit spin-triplet superconductivity, a phenomenon rarely observed. This result holds promise for a new research direction within the field of SC infinite-layer nickelates in particular and for the understanding of spin-triplet pairing in general.

We thank Brian M. Andersen, Astrid T. Rømer, Ilya M. Eremin, Frank Lechermann, Berit H. Goodge, and Matteo Dürnagel for useful discussions. Financial support by the Würzburg-Dresden Cluster of Excellence ct.qmat, EXC 2147, project ID 390858490 is gratefully acknowledged. C. Timm acknowledges funding by the Deutsche Forschungsgemeinschaft through Collaborative Research Center SFB 1143, project A04, project ID 247310070. R. Thomale and A. Consiglio acknowledge support through the SFB 1170 ToCoTronics, project ID 258499086. A. Consiglio, D. Di Sante and R. Thomale acknowledge the Gauss Centre for Supercomputing e.V. for providing computing time on the GCS Supercomputer SuperMUC at Leibniz Supercomputing Centre. D. Di Sante received funding from the European Union Horizon 2020 research and innovation program under the Marie Skłodowska-Curie Grant Agreement No. 897276. A. Consiglio acknowledges support from PNRR MUR project PE0000023-NQSTI.

* fabian.jakubczyk@tu-dresden.de

- [1] D. Li, K. Lee, B. Y. Wang, M. Osada, S. Crossley, H. R. Lee, Y. Cui, Y. Hikita, and H. Y. Hwang, Superconductivity in an infinite-layer nickelate, *Nature* **572**, 624 (2019).
- [2] M. Osada, B. Y. Wang, B. H. Goodge, S. P. Harvey, K. Lee, D. Li, L. F. Kourkoutis, and H. Y. Hwang, Nickelate Superconductivity without Rare-Earth Magnetism: $(\text{La}, \text{Sr})\text{NiO}_2$, *Adv. Mater.* **33**, 2104083 (2021).

- [3] S. Zeng, C. Li, L. E. Chow, Y. Cao, Z. Zhang, C. S. Tang, X. Yin, Z. S. Lim, J. Hu, P. Yang, and A. Ariando, Superconductivity in infinite-layer nickelate $\text{La}_{1-x}\text{Ca}_x\text{NiO}_2$ thin films, *Sci. Adv.* **8**, eabl9927 (2022).
- [4] J. Fowlie, M. Hadjimichael, M. M. Martins, D. Li, M. Osada, B. Y. Wang, K. Lee, Y. Lee, Z. Salman, T. Prokscha, J.-M. Triscone, H. Y. Hwang, and A. Suter, Intrinsic magnetism in superconducting infinite-layer nickelates, *Nat. Phys.* **18**, 1043 (2022).
- [5] W. Sun, Y. Li, R. Liu, J. Yang, J. Li, W. Wei, G. Jin, S. Yan, H. Sun, W. Guo, Z. Gu, Z. Zhu, Y. Sun, Z. Shi, Y. Deng, X. Wang, and Y. Nie, Evidence for Anisotropic Superconductivity Beyond Pauli Limit in Infinite-Layer Lanthanum Nickelates, *Adv. Mater.* **35**, 2303400 (2023).
- [6] C. T. Parzyck, Y. Wu, L. Bhatt, M. Kang, Z. Arthur, T. M. Pedersen, R. Sutarto, S. Fan, J. Pelliciani, V. Bisogni, G. Herranz, A. B. Georgescu, D. G. Hawthorn, L. F. Kourkoutis, D. A. Muller, D. G. Schlom, and K. M. Shen, Superconductivity in the parent infinite-layer nickelate NdNiO_2 , arXiv:2410.02007 (2024).
- [7] H. Sahib, F. Rosa, A. Raji, G. Merzoni, G. Ghiringhelli, M. Salluzzo, A. Gloter, N. Viart, and D. Preziosi, Superconductivity in PrNiO_2 infinite-layer nickelates, arXiv:2410.16147 (2024).
- [8] K.-W. Lee and W. E. Pickett, Infinite-layer LaNiO_2 : Ni^{1+} is not Cu^{2+} , *Phys. Rev. B* **70**, 165109 (2004).
- [9] A. Botana and M. Norman, Similarities and Differences between LaNiO_2 and CaCuO_2 and Implications for Superconductivity, *Phys. Rev. X* **10**, 011024 (2020).
- [10] F. Lechermann, Late transition metal oxides with infinite-layer structure: Nickelates versus cuprates, *Phys. Rev. B* **101**, 081110(R) (2020).
- [11] V. I. Anisimov, D. Bukhvalov, and T. M. Rice, Electronic structure of possible nickelate analogs to the cuprates, *Phys. Rev. B* **59**, 7901 (1999).
- [12] M. Hepting, D. Li, C. J. Jia, H. Lu, E. Paris, Y. Tseng, X. Feng, M. Osada, E. Been, Y. Hikita, Y.-D. Chuang, Z. Hussain, K. J. Zhou, A. Nag, M. Garcia-Fernandez, M. Rossi, H. Y. Huang, D. J. Huang, Z. X. Shen, T. Schmitt, H. Y. Hwang, B. Moritz, J. Zaanen, T. P. Devereaux, and W. S. Lee, Electronic structure of the parent compound of superconducting infinite-layer nickelates, *Nat. Mater.* **19**, 381 (2020).
- [13] B. Y. Wang, D. Li, B. H. Goodge, K. Lee, M. Osada, S. P. Harvey, L. F. Kourkoutis, M. R. Beasley, and H. Y. Hwang, Isotropic Pauli-limited superconductivity in the infinite-layer nickelate $\text{Nd}_{0.775}\text{Sr}_{0.225}\text{NiO}_2$, *Nat. Phys.* **17**, 473 (2021).
- [14] H. Sakakibara, H. Usui, K. Suzuki, T. Kotani, H. Aoki, and K. Kuroki, Model Construction and a Possibility of Cupratelike Pairing in a New d^9 Nickelate Superconductor $(\text{Nd,Sr})\text{NiO}_2$, *Phys. Rev. Lett.* **125**, 077003 (2020).
- [15] X. Wu, D. Di Sante, T. Schwemmer, W. Hanke, H. Y. Hwang, S. Raghu, and R. Thomale, Robust $d_{x^2-y^2}$ -wave superconductivity of infinite-layer nickelates, *Phys. Rev. B* **101**, 060504(R) (2020).
- [16] M. Kitatani, L. Si, O. Janson, R. Arita, Z. Zhong, and K. Held, Nickelate superconductors - a renaissance of the one-band Hubbard model, *npj Quantum Mater.* **5**, 59 (2020).
- [17] P. Adhikary, S. Bandyopadhyay, T. Das, I. Dasgupta, and T. Saha-Dasgupta, Orbital-selective superconductivity in a two-band model of infinite-layer nickelates, *Phys. Rev. B* **102**, 100501(R) (2020).
- [18] T. Y. Xie, Z. Liu, C. Cao, Z. F. Wang, J. L. Yang, and W. Zhu, Microscopic theory of superconducting phase diagram in infinite-layer nickelates, *Phys. Rev. B* **106**, 035111 (2022).
- [19] C. Lu, L.-H. Hu, Y. Wang, F. Yang, and C. Wu, Two-orbital model for possible superconductivity pairing mechanism in nickelates, *Phys. Rev. B* **105**, 054516 (2022).
- [20] L. E. Chow, K. Y. Yip, M. Pierre, S. W. Zeng, Z. T. Zhang, T. Heil, J. Deuschle, P. Nandi, Z. S. Lim, Z. Y. Luo, M. Nardone, A. Zitouni, P. A. van Aken, M. Goiran, S. K. Goh, and A. Ariando, Pauli-limit violation in lanthanide infinite-layer nickelate superconductors, arXiv:2204.12606 (2022).
- [21] W. Wei, W. Sun, Y. Sun, Y. Pan, G. Jin, F. Yang, Y. Li, Z. Zhu, Y. Nie, and Z. Shi, Large upper critical fields and dimensionality crossover of superconductivity in the infinite-layer nickelate $\text{La}_{0.8}\text{Sr}_{0.2}\text{NiO}_2$, *Phys. Rev. B* **107**, L220503 (2023).
- [22] S. Yan, W. Mao, W. Sun, Y. Li, H. Sun, J. Yang, B. Hao, W. Guo, L. Nian, Z. Gu, P. Wang, and Y. Nie, Superconductivity in freestanding infinite-layer nickelate membranes, arXiv:2401.15980 (2024).
- [23] B. Y. Wang, T. C. Wang, Y.-T. Hsu, M. Osada, K. Lee, C. Jia, C. Duffy, D. Li, J. Fowlie, M. R. Beasley, T. P. Devereaux, I. R. Fisher, N. E. Hussey, and H. Y. Hwang, Effects of rare-earth magnetism on the superconducting upper critical field in infinite-layer nickelates, *Sci. Adv.* **9**, eadf6655 (2023).
- [24] M.-Y. Choi, K.-W. Lee, and W. E. Pickett, Role of $4f$ states in infinite-layer NdNiO_2 , *Phys. Rev. B* **101**, 020503(R) (2020).
- [25] R. Zhang, C. Lane, B. Singh, J. Nokelainen, B. Barbiellini, R. S. Markiewicz, A. Bansil, and J. Sun, Magnetic and f -electron effects in LaNiO_2 and NdNiO_2 nickelates with cuprate-like $3d_{x^2-y^2}$ band, *Commun. Phys.* **4**, 118 (2021).
- [26] P. Jiang, L. Si, Z. Liao, and Z. Zhong, Electronic structure of rare-earth infinite-layer RNiO_2 ($R = \text{La}, \text{Nd}$), *Phys. Rev. B* **100**, 201106(R) (2019).
- [27] S. Bandyopadhyay, P. Adhikary, T. Das, I. Dasgupta, and T. Saha-Dasgupta, Superconductivity in infinite-layer nickelates: Role of f orbitals, *Phys. Rev. B* **102**, 220502(R) (2020).
- [28] D. J. Scalapino, A common thread: The pairing interaction for unconventional superconductors, *Rev. Mod. Phys.* **84**, 1383 (2012).
- [29] Y. Yamakawa, S. Onari, and H. Kontani, Nematicity and Magnetism in FeSe and Other Families of Fe-Based Superconductors, *Phys. Rev. X* **6**, 021032 (2016).
- [30] A. Kreisel, B. M. Andersen, P. O. Sprau, A. Kostin, J. C. S. Davis, and P. J. Hirschfeld, Orbital selective pairing and gap structures of iron-based superconductors, *Phys. Rev. B* **95**, 174504 (2017).
- [31] H. Lin, D. J. Gawryluk, Y. M. Klein, S. Huangfu, E. Pomjakushina, F. von Rohr, and A. Schilling, Universal spin-glass behaviour in bulk LaNiO_2 , PrNiO_2 and NdNiO_2 , *New J. Phys.* **24**, 013022 (2022).
- [32] R. A. Ortiz, P. Puphal, M. Klett, F. Hotz, R. K. Kremer, H. Trepka, M. Hemmida, H.-A. Krug von Nidda, M. Isobe, R. Khasanov, H. Luetkens, P. Hansmann, B. Keimer, T. Schäfer, and M. Hepting, Magnetic correlations in infinite-layer nickelates: An experimental and theoretical multimethod study, *Phys. Rev. Res.* **4**, 023093 (2022).

- (2022).
- [33] D. Zhao, Y. Zhou, Y. Fu, L. Wang, X. Zhou, H. Cheng, J. Li, D. Song, S. Li, B. Kang, L. Zheng, L. Nie, Z. Wu, M. Shan, F. Yu, J. Ying, S. Wang, J. Mei, T. Wu, and X. Chen, Intrinsic Spin Susceptibility and Pseudogaplike Behavior in Infinite-Layer LaNiO_2 , *Phys. Rev. Lett.* **126**, 197001 (2021).
 - [34] F. Lechermann, Assessing the correlated electronic structure of lanthanum nickelates, *Electron. Struct.* **4**, 015005 (2022).
 - [35] C.-J. Kang and G. Kotliar, Optical Properties of the Infinite-Layer $\text{La}_{1-x}\text{Sr}_x\text{NiO}_2$ and Hidden Hund's Physics, *Phys. Rev. Lett.* **126**, 127401 (2021).
 - [36] J. Kapeghian and A. S. Botana, Electronic structure and magnetism in infinite-layer nickelates RNiO_2 ($R = \text{La} - \text{Lu}$), *Phys. Rev. B* **102**, 205130 (2020).
 - [37] Y. Wang, C.-J. Kang, H. Miao, and G. Kotliar, Hund's metal physics: From SrNiO_2 to LaNiO_2 , *Phys. Rev. B* **102**, 161118(R) (2020).
 - [38] H. Lu, M. Rossi, A. Nag, M. Osada, D. F. Li, K. Lee, B. Y. Wang, M. Garcia-Fernandez, S. Agrestini, Z. X. Shen, E. M. Been, B. Moritz, T. P. Devereaux, J. Zaanen, H. Y. Hwang, K.-J. Zhou, and W. S. Lee, Magnetic excitations in infinite-layer nickelates, *Science* **373**, 213 (2021).
 - [39] A. Kreisel, B. M. Andersen, A. T. Rømer, I. M. Eremin, and F. Lechermann, Superconducting Instabilities in Strongly Correlated Infinite-Layer Nickelates, *Phys. Rev. Lett.* **129**, 077002 (2022).
 - [40] P. Worm, Q. Wang, M. Kitatani, I. Biało, Q. Gao, X. Ren, J. Choi, D. Csontosová, K.-J. Zhou, X. Zhou, Z. Zhu, L. Si, J. Chang, J. M. Tomczak, and K. Held, Spin fluctuations sufficient to mediate superconductivity in nickelates, *arXiv:2312.08260* (2023).
 - [41] R. A. Shi, B. Y. Wang, Y. Iguchi, M. Osada, K. Lee, B. H. Goodge, L. F. Kourkoutis, H. Y. Hwang, and K. A. Moler, Scanning SQUID study of ferromagnetism and superconductivity in infinite-layer nickelates, *Phys. Rev. Mater.* **8**, 024802 (2024).
 - [42] W. Sun, Z. Jiang, C. Xia, B. Hao, Y. Li, S. Yan, M. Wang, H. Liu, J. Ding, J. Liu, Z. Liu, J. Liu, H. Chen, D. Shen, and Y. Nie, Title: Electronic structure of superconducting infinite-layer lanthanum nickelates, *arxiv:2403.07344* (2024).
 - [43] P. Werner and S. Hoshino, Nickelate superconductors: Multiorbital nature and spin freezing, *Phys. Rev. B* **101**, 041104(R) (2020).
 - [44] J. Krishna, H. LaBollita, A. O. Fumega, V. Pardo, and A. S. Botana, Effects of Sr doping on the electronic and spin-state properties of infinite-layer nickelates: Nature of holes, *Phys. Rev. B* **102**, 224506 (2020).
 - [45] I. Leonov, S. L. Skornyakov, and S. Y. Savrasov, Lifshitz transition and frustration of magnetic moments in infinite-layer NdNiO_2 upon hole doping, *Phys. Rev. B* **101**, 241108(R) (2020).
 - [46] C. Lane, R. Zhang, B. Barbiellini, R. S. Markiewicz, A. Bansil, J. Sun, and J.-X. Zhu, Competing incommensurate spin fluctuations and magnetic excitations in infinite-layer nickelate superconductors, *Commun. Phys.* **6**, 90 (2023).
 - [47] Z. Liu, Z. Ren, W. Zhu, Z. Wang, and J. Yang, Electronic and magnetic structure of infinite-layer NdNiO_2 : trace of antiferromagnetic metal, *npj Quantum Mater.* **5**, 31 (2020).
 - [48] V. Olevano, F. Bernardini, X. Blase, and A. Cano, *Ab initio* many-body GW correlations in the electronic structure of LaNiO_2 , *Phys. Rev. B* **101**, 161102(R) (2020).
 - [49] See supplemental material at <http://link.aps.org/...> for additional information about the ab-initio calculations, derivations of the renormalized superconducting pairing, and results for doped LaNiO_2 , which includes Refs. [29, 30, 55, 57, 59, 70–87].
 - [50] S. Ryee, H. Yoon, T. J. Kim, M. Y. Jeong, and M. J. Han, Induced magnetic two-dimensionality by hole doping in the superconducting infinite-layer nickelate $\text{Nd}_{1-x}\text{Sr}_x\text{NiO}_2$, *Phys. Rev. B* **101**, 064513 (2020).
 - [51] L. Si, W. Xiao, J. Kaufmann, J. M. Tomczak, Y. Lu, Z. Zhong, and K. Held, Topotactic Hydrogen in Nickelate Superconductors and Akin Infinite-Layer Oxides ABO_2 , *Phys. Rev. Lett.* **124** (2020).
 - [52] K. Kubo, Pairing symmetry in a two-orbital Hubbard model on a square lattice, *Phys. Rev. B* **75**, 224509 (2007).
 - [53] H. Tang, M. Plihal, and D. L. Mills, Theory of the spin dynamics of bulk Fe and ultrathin Fe(100) films, *J. Magn. Magn. Mater.* **187**, 23 (1998).
 - [54] B. Kang, C. Melnick, P. Semon, S. Ryee, M. J. Han, G. Kotliar, and S. Choi, Infinite-layer nickelates as Ni- e_g Hund's metals, *npj Quantum Mater.* **8**, 35 (2023).
 - [55] A. T. Rømer, A. Kreisel, I. M. Eremin, M. A. Malakhov, T. A. Maier, P. J. Hirschfeld, and B. M. Andersen, Pairing symmetry of the one-band hubbard model in the paramagnetic weak-coupling limit: A numerical RPA study, *Phys. Rev. B* **92**, 104505 (2015).
 - [56] N. F. Berk and J. R. Schrieffer, Effect of Ferromagnetic Spin Correlations on Superconductivity, *Phys. Rev. Lett.* **17**, 433 (1966).
 - [57] S. Graser, T. A. Maier, P. J. Hirschfeld, and D. J. Scalapino, Near-degeneracy of several pairing channels in multiorbital models for the Fe pnictides, *New J. Phys.* **11**, 025016 (2009).
 - [58] A. Kreisel, Y. Wang, T. A. Maier, P. J. Hirschfeld, and D. J. Scalapino, Spin fluctuations and superconductivity in $\text{K}_x\text{Fe}_{2-y}\text{Se}_2$, *Phys. Rev. B* **88**, 094522 (2013).
 - [59] D. J. Scalapino, E. Loh, and J. E. Hirsch, d -wave pairing near a spin-density-wave instability, *Phys. Rev. B* **34**, 8190 (1986).
 - [60] M. Dürrnagel, J. Beyer, R. Thomale, and T. Schwemmer, Unconventional superconductivity from weak coupling: A unified perspective on formalism and numerical implementation, *Eur. Phys. J. B* **95**, 112 (2022).
 - [61] M. Sigrist, Introduction to Unconventional Superconductivity, *AIP Conf. Proc.* **789**, 165 (2005).
 - [62] A. P. Mackenzie and Y. Maeno, The superconductivity of Sr_2RuO_4 and the physics of spin-triplet pairing, *Rev. Mod. Phys.* **75**, 657 (2003).
 - [63] J. W. Serene, The superfluid phases of helium 3, *Science* **251**, 97 (1991).
 - [64] M. Sigrist and K. Ueda, Phenomenological theory of unconventional superconductivity, *Rev. Mod. Phys.* **63**, 239 (1991).
 - [65] J. F. Annett, B. L. Györfy, and K. I. Wysokiński, Orbital magnetic moment of a chiral p -wave superconductor, *New J. Phys.* **11**, 055063 (2009).
 - [66] M. P. Smylie, H. Claus, U. Welp, W.-K. Kwok, Y. Qiu, Y. S. Hor, and A. Snezhko, Evidence of nodes in the order parameter of the superconducting doped topological insulator $\text{Nb}_x\text{Bi}_2\text{Se}_3$ via penetration depth measurements,

- Phys. Rev. B **94**, 180510(R) (2016).
- [67] R. T. Gordon, C. Martin, H. Kim, N. Ni, M. A. Tanatar, J. Schmalian, I. I. Mazin, S. L. Bud'ko, P. C. Canfield, and R. Prozorov, London penetration depth in single crystals of $\text{Ba}(\text{Fe}_{1-x}\text{Co}_x)_2\text{As}_2$ spanning underdoped to overdoped compositions, Phys. Rev. B **79**, 100506(R) (2009).
 - [68] S. P. Harvey, B. Y. Wang, J. Fowlie, M. Osada, K. Lee, Y. Lee, D. Li, and H. Y. Hwang, Evidence for nodal superconductivity in infinite-layer nickelates, arXiv:2201.12971 (2022).
 - [69] L. E. Chow, S. K. Sudheesh, Z. Y. Luo, P. Nandi, T. Heil, J. Deuschle, S. W. Zeng, Z. T. Zhang, S. Prakash, X. M. Du, Z. S. Lim, P. A. van Aken, E. E. M. Chia, and A. Ariando, Pairing symmetry in infinite-layer nickelate superconductors, arXiv:2201.10038 (2023).
 - [70] G. Kresse and D. Joubert, From ultrasoft pseudopotentials to the projector augmented-wave method, Phys. Rev. B **59**, 1758 (1999).
 - [71] G. Kresse and J. Furthmüller, Efficient iterative schemes for ab initio total-energy calculations using a plane-wave basis set, Phys. Rev. B **54**, 11169 (1996).
 - [72] J. P. Perdew, J. A. Chevary, S. H. Vosko, K. A. Jackson, M. R. Pederson, D. J. Singh, and C. Fiolhais, Atoms, molecules, solids, and surfaces: Applications of the generalized gradient approximation for exchange and correlation, Phys. Rev. B **46**, 6671 (1992).
 - [73] A. D. Becke, Density-functional exchange-energy approximation with correct asymptotic behavior, Phys. Rev. A **38**, 3098 (1988).
 - [74] D. C. Langreth and M. J. Mehl, Beyond the local-density approximation in calculations of ground-state electronic properties, Phys. Rev. B **28**, 1809 (1983).
 - [75] P. E. Blöchl, Projector augmented-wave method, Phys. Rev. B **50**, 17953 (1994).
 - [76] J. P. Perdew, K. Burke, and M. Ernzerhof, Generalized gradient approximation made simple, Phys. Rev. Lett. **77**, 3865 (1996).
 - [77] G. H. Wannier, The structure of electronic excitation levels in insulating crystals, Phys. Rev. **52**, 191 (1937).
 - [78] G. H. Wannier, Dynamics of band electrons in electric and magnetic fields, Rev. Mod. Phys. **34**, 645 (1962).
 - [79] A. A. Mostofi, J. R. Yates, G. Pizzi, Y.-S. Lee, I. Souza, D. Vanderbilt, and N. Marzari, An updated version of wannier90: A tool for obtaining maximally-localised wannier functions, Comp. Phys. Commun. **185**, 2309 (2014).
 - [80] N. Marzari, A. A. Mostofi, J. R. Yates, I. Souza, and D. Vanderbilt, Maximally localized wannier functions: Theory and applications, Rev. Mod. Phys. **84**, 1419 (2012).
 - [81] N. Marzari and D. Vanderbilt, Maximally localized generalized wannier functions for composite energy bands, Phys. Rev. B **56**, 12847 (1997).
 - [82] I. Souza, N. Marzari, and D. Vanderbilt, Maximally localized wannier functions for entangled energy bands, Phys. Rev. B **65**, 035109 (2001).
 - [83] V. Wang, N. Xu, J.-C. Liu, G. Tang, and W.-T. Geng, Vaspkit: A user-friendly interface facilitating high-throughput computing and analysis using vasp code, Comp. Phys. Commun. **267**, 108033 (2021).
 - [84] K. Momma and F. Izumi, *VESTA*: a three-dimensional visualization system for electronic and structural analysis, Journ. Appl. Cryst. **41**, 653 (2008).
 - [85] A. F. Kemper, T. A. Maier, S. Graser, H.-P. Cheng, P. J. Hirschfeld, and D. J. Scalapino, Sensitivity of the superconducting state and magnetic susceptibility to key aspects of electronic structure in ferropnictides, New J. Phys. **12**, 073030 (2010).
 - [86] G. Heier, K. Park, and S. Y. Savrasov, Competing d_{xy} and s_{\pm} pairing symmetries in superconducting $\text{La}_3\text{Ni}_2\text{O}_7$: LDA + FLEX calculations, Phys. Rev. B **109**, 104508 (2024).
 - [87] Y.-B. Liu, J.-W. Mei, F. Ye, W.-Q. Chen, and F. Yang, s_{\pm} -Wave Pairing and the Destructive Role of Apical-Oxygen Deficiencies in $\text{La}_3\text{Ni}_2\text{O}_7$ under Pressure, Phys. Rev. Lett. **131**, 236002 (2023).

Supplemental Material: Orbital-Selective Spin-Triplet Superconductivity in Infinite-Layer LaNiO_2

Fabian Jakubczyk,^{1,2,*} Armando Consiglio,^{2,3,4} Domenico Di Sante,⁵ Ronny Thomale,^{2,3} and Carsten Timm^{1,2}

¹*Institute of Theoretical Physics, Technische Universität Dresden, 01069 Dresden, Germany*

²*Würzburg-Dresden Cluster of Excellence ct.qmat, Germany*

³*Institut für Theoretische Physik und Astrophysik, Universität Würzburg, 97074 Würzburg, Germany*

⁴*Istituto Officina dei Materiali, Consiglio Nazionale delle Ricerche, Trieste I-34149, Italy*

⁵*Department of Physics and Astronomy, University of Bologna, 40127 Bologna, Italy*

(Dated: December 4, 2024)

I. DFT ELECTRONIC STRUCTURE

DFT calculations have been performed using the Vienna ab-initio Simulation Package (VASP) [1, 2], employing the projector augmented wave (PAW) method [3]. Exchange and correlation effects have been handled using the generalized gradient approximation (GGA) [4–6] within the Perdew-Burke-Ernzerhof (PBE) approach [7]. A plane-wave cutoff of 500 eV was used for the truncation of the basis set, while the relaxation of the electronic and ionic degrees of freedom was considered converged when the output difference between two steps was equal or smaller than 1×10^{-6} eV and 1×10^{-8} eV/Å, respectively. The chosen number of k-points is $16 \times 16 \times 16$. Partial occupancies have been determined via Gaussian smearing with a width of 0.1 eV. Spin-orbit coupling (SOC) has generally not been considered, unless stated otherwise, in which case SOC has been included self-consistently. The comparison between the cases with and without SOC is shown in Fig. S1(d).

In our DFT single-particle calculations, the paramagnetic phase of LaNiO_2 has been modeled by neglecting the spin-polarization degree of freedom. To justify this approach, and verify that the non-magnetic configuration accurately describes a paramagnetic state, we study several supercells configurations ($2 \times 2 \times 3$ expansions of the original unit cell) within the disordered local moment framework, i.e. assigning random magnetic moments to the Ni sites and ensuring that the total magnetic moment sums up to zero. This setup approximates the behavior of a real paramagnetic material. As shown in Fig. S2(b) to S2(f), the unfolded electronic band structures from several such magnetic configurations, subject to the constraints defined above, closely align with the results obtained from non-magnetic DFT calculations (Fig. S2(a)). This agreement supports the validity of the non-magnetic approximation for the paramagnetic state and its subsequent use in many-body analysis. For the purposes of the present work, the terms “non-magnetic” and “paramagnetic” can be considered as interchangeable and synonymous.

Starting from the non-magnetic system and its corresponding electronic structure, Wannier functions [8, 9] have been used to provide an equivalent description of Bloch states via a maximally localized orbital basis. The Wannier-basis position matrix elements $\langle 0n|\hat{r}|Rm\rangle$, Rm being the maximally-localized Wannier function m in unit cell R , have been used for the tight-binding

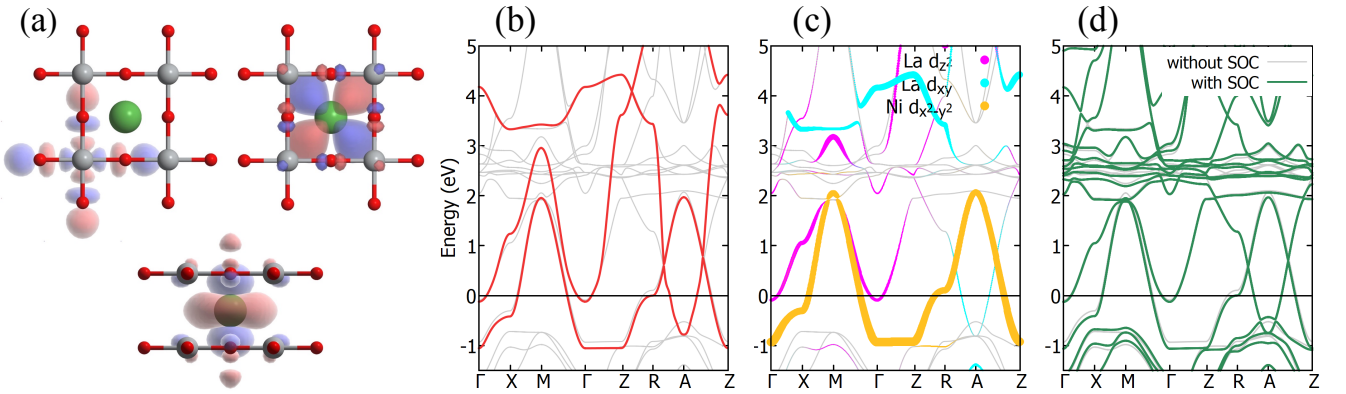


FIG. S1. (a) Isosurfaces of the Wannier orbitals used for the three-band model. The upper left and right panels show top views of the Ni $d_{x^2-y^2}$ and La d_{xy} Wannier orbitals, respectively. The lower panel shows a side view of the La d_{z^2} orbital. (b) Comparison between DFT band structure (gray lines) and bands derived from the three-band Wannier model (red lines). (c) DFT band structure projected onto the three orbitals of the model: La d_{z^2} , La d_{xy} , and Ni $d_{x^2-y^2}$. (d) Comparison between DFT band structures, with and without SOC.

* fabian.jakubczyk@tu-dresden.de

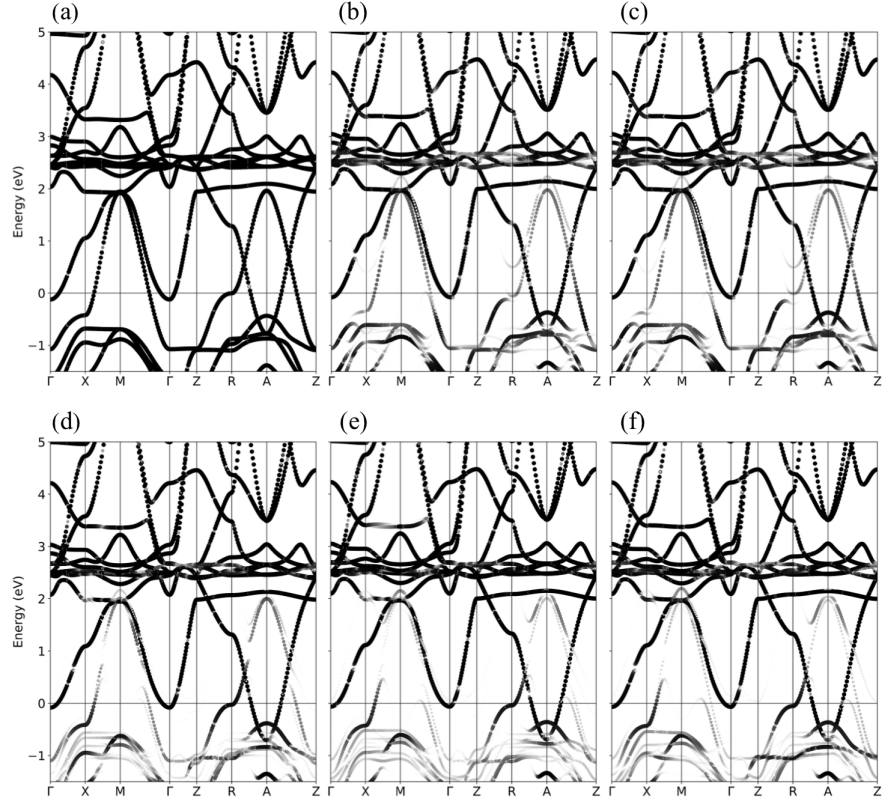


FIG. S2. Electronic band structures of LaNiO_2 at DFT level in several paramagnetic configurations. The weight of the dots represents the contribution of the supercell eigenstate in the primitive BZ. (a) Electronic structure of the pristine unit cell without magnetism. (b)–(f) Electronic structures of some magnetic supercells with average zero magnetization, unfolded in the primitive BZ.

(TB) description, as shown in Figs. S1(a) and S1(b) [10–13]. For the three-band model, the projection functions used to build the initial guess $A(\mathbf{k})_{mn} = \langle \psi_{m\mathbf{k}} | g_n \rangle$ for the unitary transformation are provided by Ni $d_{x^2-y^2}$, La d_{xy} , and La d_{z^2} orbitals. $|g_n\rangle$ represents the trial localized orbitals, and $|\psi_{m\mathbf{k}}\rangle$ are the Bloch states. DFT band structures have been visualized using the VASPKIT postprocessing tool, as shown in Fig. S1(c) [14], while VESTA [15] has been used to visualize the Wannier-orbital isosurfaces and crystal structures in Fig. S1(a).

II. WANNIER HAMILTONIAN

We introduce the operator $\psi_\sigma^\dagger(\mathbf{k}) = [c_{1\sigma}^\dagger(\mathbf{k}), c_{2\sigma}^\dagger(\mathbf{k}), c_{3\sigma}^\dagger(\mathbf{k})]$ to describe the given multiband system. Here, $c_{l\sigma}^\dagger(\mathbf{k})$ is the fermionic creation operator, where σ and l denote the spin and orbital index, with $l = 1, 2, 3$ referring to the La $5d_{z^2}$, La $5d_{xy}$, and Ni $3d_{x^2-y^2}$ orbital, respectively. We thus write the non-interacting Hamiltonian as

$$H_0 = \sum_{\mathbf{k}\sigma} \psi_\sigma^\dagger(\mathbf{k}) h(\mathbf{k}) \psi_\sigma(\mathbf{k}). \quad (\text{S1})$$

For the derivation of the matrix elements in the Hamiltonian $h(\mathbf{k})$ we employ an energy cutoff of 0.01 eV for the TB hopping amplitudes. The Hamiltonian is given by

$$\begin{aligned} h_{11} &= \epsilon_1 - \mu + 2t_{11}^x (\cos k_x + \cos k_y) + 2t_{11}^{xx} (\cos 2k_x + \cos 2k_y) + 2t_{11}^z \cos k_z + 2t_{11}^{zz} \cos 2k_z \\ &\quad + 4t_{11}^{xz} \cos 2k_z (\cos k_x + \cos k_y), \\ h_{22} &= \epsilon_2 - \mu + 2t_{22}^x (\cos k_x + \cos k_y) + 4t_{22}^{xy} \cos k_x \cos k_y + 2t_{22}^{xx} (\cos 2k_x + \cos 2k_y) \\ &\quad + 4t_{22}^{xy} (\cos 2k_x \cos k_y + \cos k_x \cos 2k_y) + 2t_{22}^z \cos k_z + 2t_{22}^{zz} \cos 2k_z \\ &\quad + 4t_{22}^{xz} \cos k_z (\cos k_x + \cos k_y) + 8t_{22}^{xyz} \cos k_x \cos k_y \cos k_z + 4t_{22}^{xxz} \cos k_z (\cos 2k_x + \cos 2k_y) \end{aligned} \quad (\text{S2})$$

$$\begin{aligned}
& + 8t_{22}^{xyz} \cos k_z (\cos 2k_x \cos k_y + \cos k_x \cos 2k_y) + 2t_{22}^{zzz} \cos(3k_z) \\
& + 4t_{22}^{zzz} \cos 2k_z (\cos k_x + \cos k_y) + 4t_{22}^{xxx} \cos 2k_z (\cos 2k_x + \cos 2k_y) \\
& + 8t_{22}^{xyz} \cos 2k_z (\cos 2k_x \cos k_y + \cos k_x \cos 2k_y),
\end{aligned} \tag{S3}$$

$$\begin{aligned}
h_{33} = & \epsilon_3 - \mu + 2t_{33}^x (\cos k_x + \cos k_y) + 4t_{33}^{xy} \cos k_x \cos k_y + 2t_{33}^{xx} (\cos 2k_x + \cos 2k_y) + 2t_{33}^z \cos k_z \\
& + 8t_{33}^{xyz} \cos k_x \cos k_y \cos k_z,
\end{aligned} \tag{S4}$$

$$h_{12} = -4t_{12}^{xy} \sin k_x \sin k_y - 8t_{12}^{xyz} \sin k_x \sin k_y \cos k_z - 8t_{12}^{xyzz} \sin k_x \sin k_y \cos 2k_z, \tag{S5}$$

$$\begin{aligned}
h_{13} = & 8t_{13}^x (\cos 3/2k_x \cos 1/2k_y - \cos 1/2k_x \cos 3/2k_y) \cos 1/2k_z \\
& + 8t_{13}^{xz} (\cos 3/2k_x \cos 1/2k_y - \cos 1/2k_x \cos 3/2k_y) \cos 3/2k_z,
\end{aligned} \tag{S6}$$

$$\begin{aligned}
h_{23} = & -8t_{23}^x (\sin 3/2k_x \sin 1/2k_y - \sin 1/2k_x \sin 3/2k_y) \cos 1/2k_z \\
& - 8t_{23}^{xz} (\sin 3/2k_x \sin 1/2k_y - \sin 1/2k_x \sin 3/2k_y) \cos 3/2k_z.
\end{aligned} \tag{S7}$$

We use a chemical potential of $\mu = 9.28$ eV and $\mu = 9.12$ eV in the undoped and doped scenario, respectively. The corresponding TB parameters specified in units of eV are

$$\epsilon_1 = 12.3837, \epsilon_2 = 12.3325, \epsilon_3 = 9.6706, \tag{S8}$$

$$t_{11}^x = -0.4266, t_{11}^{xx} = 0.0401, t_{11}^z = -1.0314, t_{11}^{zz} = 0.1150, t_{11}^{zzz} = 0.0155, \tag{S9}$$

$$t_{22}^x = 0.3964, t_{22}^{xy} = -0.0602, t_{22}^{xx} = 0.0417, t_{22}^z = 0.3545, t_{22}^{zz} = -0.1680, t_{22}^{xyz} = 0.0571,$$

$$\begin{aligned}
& t_{22}^{zzz} = -0.0549, t_{22}^{xxx} = -0.0242, t_{22}^{xyx} = -0.0230, t_{22}^{xyyz} = 0.0210, t_{22}^{zzz} = 0.0113, \\
& t_{22}^{xxx} = 0.0144, t_{22}^{xyz} = 0.0103, t_{22}^{xyzz} = -0.0107,
\end{aligned} \tag{S10}$$

$$t_{33}^x = -0.3656, t_{33}^{xy} = 0.0941, t_{33}^{xx} = -0.0441, t_{33}^z = -0.0413, t_{33}^{xyz} = 0.0121, \tag{S11}$$

$$t_{12}^{xy} = 0.0777, t_{12}^{xyz} = -0.0541, t_{12}^{xyzz} = 0.0100, \tag{S12}$$

$$t_{13}^x = 0.0277, t_{13}^{xz} = -0.0142, \tag{S13}$$

$$t_{23}^x = -0.0183, t_{23}^{xz} = 0.0198. \tag{S14}$$

The density of states (DOS) of the unrenormalized system can be obtained from

$$\rho(\omega_n) = -\frac{1}{N\pi} \sum_k \text{Im Tr}[(i\omega_n \mathbb{1} - h(\mathbf{k}))^{-1}]. \tag{S15}$$

III. RENORMALIZED SUSCEPTIBILITIES AND SUPERCONDUCTING PAIRING

Within the orbital selective ansatz [16, 17], quasiparticles in orbital l are weighted by a factor $\sqrt{Z_l}$, i.e., $c_l^\dagger(\mathbf{k}) \rightarrow \sqrt{Z_l} c_l^\dagger(\mathbf{k})$, such that the Green's function in the orbital basis $G_{ll'}(\mathbf{k}, \omega_n)$ becomes

$$\tilde{G}_{ll'}(\mathbf{k}, \omega_n) = \sqrt{Z_l Z_{l'}} \sum_\mu \frac{a_\mu^l(\mathbf{k}) a_{\mu'}^{l'*}(\mathbf{k})}{i\omega_n - E_\mu(\mathbf{k})}, \tag{S16}$$

where $E_\mu(\mathbf{k})$ is the eigenenergy of band μ . The renormalized Green's function enters the bare (non-interacting) susceptibilities, which after performing Matsubara-frequency summation read as

$$\tilde{\chi}_{l_1 l_2 l_3 l_4}^0(\mathbf{q}, \omega) = -\frac{1}{N} \sum_{k, \mu\nu} \tilde{\eta}_{\mu\nu}(\mathbf{k}, \mathbf{q}) \frac{n_F(E_\nu(\mathbf{k} + \mathbf{q})) - n_F(E_\mu(\mathbf{k}))}{E_\nu(\mathbf{k} + \mathbf{q}) - E_\mu(\mathbf{k}) + \omega + i0^+}, \tag{S17}$$

with the Fermi-Dirac distribution n_F . Here, we have absorbed the quasiparticle weights into the dressing factor

$$\tilde{\eta}_{\mu\nu}(\mathbf{k}, \mathbf{q}) = \sqrt{Z_{l_1} Z_{l_2} Z_{l_3} Z_{l_4}} a_\mu^{l_4}(\mathbf{k}) a_{\mu'}^{l_2*}(\mathbf{k}) a_\nu^{l_1}(\mathbf{k} + \mathbf{q}) a_{\nu'}^{l_3*}(\mathbf{k} + \mathbf{q}), \tag{S18}$$

and $a_\mu^l(\mathbf{k})$ is the matrix element of the unitary transformation that connects band μ to orbital l . The homogeneous or physical bare spin susceptibility can be calculated by performing the sum

$$\tilde{\chi}_{\text{phys}}^0(\mathbf{q}) = \frac{1}{2} \sum_{ll'} \tilde{\chi}_{ll' l' l}^0(\mathbf{q}, 0) \tag{S19}$$

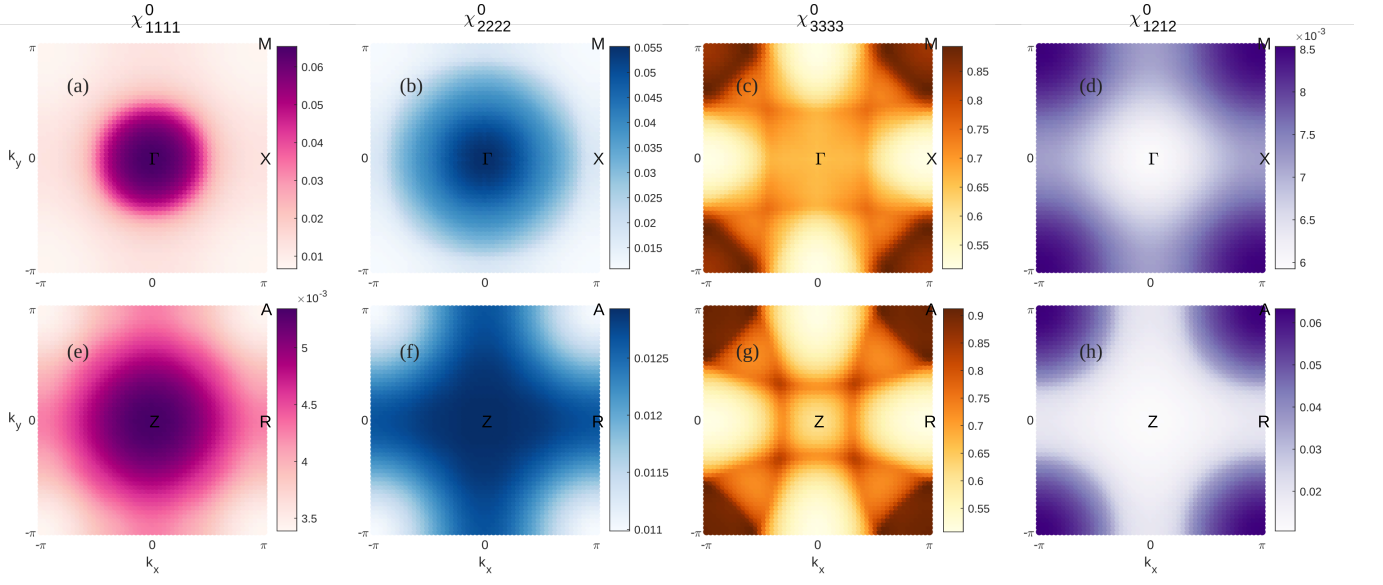


FIG. S3. Static ($\omega = 0$) bare susceptibilities of pristine LaNiO_2 for $Z_{d_{x^2-y^2}} = 1$ in the k_x k_y -plane for (a) - (d) $k_z = 0$ and (e) - (h) $k_z = \pi$. In panels (a), (e) $\tilde{\chi}_{1111}^0$, (b), (f) $\tilde{\chi}_{2222}^0$, and (c), (g) $\tilde{\chi}_{3333}^0$ represent the diagonal La d_{z^2} , La d_{xy} , and Ni $d_{x^2-y^2}$ orbital contributions, respectively. Moreover, we show the interorbital susceptibility $\tilde{\chi}_{1212}^0$ in panels (d) and (h). Momentum-space integration is done on a mesh of $60 \times 60 \times 60$ \mathbf{k} -points.

of the static ($\omega = 0$) susceptibility [18]. In Fig. S3, we show plots of the bare susceptibilities $\tilde{\chi}_{1111}^0$, $\tilde{\chi}_{2222}^0$, $\tilde{\chi}_{3333}^0$, and $\tilde{\chi}_{1212}^0$ obtained for undoped LaNiO_2 without renormalization along 2D cuts ($k_z = 0, \pi$) through the Brillouin zone (BZ). Especially the $\tilde{\chi}_{3333}^0$ component shows nesting features familiar from the cuprates [19]. However, quasiparticle renormalization strongly dampens these features, such that they become less significant in the renormalized case. Note that for instance the interorbital susceptibility contribution $\tilde{\chi}_{1212}^0$ would not be observable within the physical susceptibility given in Eq. (S19).

Interactions are included in the calculation of susceptibilities within the random phase approximation (RPA). The spin-fluctuation and charge-fluctuation parts of the susceptibility are then given by [20]

$$\tilde{\chi}_{l_1 l_2 l_3 l_4}^{\text{RPA}, s}(\mathbf{q}, \omega) = \{\tilde{\chi}^0(\mathbf{q}, \omega)[\mathbb{1} - U^s \tilde{\chi}^0(\mathbf{q}, \omega)]\}_{l_1 l_2 l_3 l_4}^{-1}, \quad (\text{S20})$$

$$\tilde{\chi}_{l_1 l_2 l_3 l_4}^{\text{RPA}, c}(\mathbf{q}, \omega) = \{\tilde{\chi}^0(\mathbf{q}, \omega)[\mathbb{1} + U^c \tilde{\chi}^0(\mathbf{q}, \omega)]\}_{l_1 l_2 l_3 l_4}^{-1}. \quad (\text{S21})$$

In orbital space, the spin and charge interaction matrices U^s and U^c containing the interaction parameters are given by

$$U_{l_1 l_2 l_3 l_4}^s = \begin{cases} U_\tau, & l_1 = l_2 = l_3 = l_4, \\ U'_\tau, & l_1 = l_3 \neq l_2 = l_4, \\ J_\tau, & l_1 = l_2 \neq l_3 = l_4, \\ J'_\tau, & l_1 = l_4 \neq l_2 = l_3, \end{cases} \quad (\text{S22})$$

$$U_{l_1 l_2 l_3 l_4}^c = \begin{cases} U_\tau, & l_1 = l_2 = l_3 = l_4, \\ -U'_\tau + 2J_\tau, & l_1 = l_3 \neq l_2 = l_4, \\ 2U'_\tau - J_\tau, & l_1 = l_2 \neq l_3 = l_4, \\ J'_\tau, & l_1 = l_4 \neq l_2 = l_3, \end{cases} \quad (\text{S23})$$

respectively, where $\tau \in (\text{La}, \text{Ni})$ is the sublattice index.

In order to determine the superconducting (SC) pairing symmetries, we solve the linearized gap equation

$$\lambda_\alpha f_\alpha(\mathbf{k}) = \sum_j \oint_{C_j} \frac{d^2 k'_\parallel}{(2\pi)^2 v_F(\mathbf{k}')} \tilde{\Gamma}_{ij}(\mathbf{k}, \mathbf{k}') f_\alpha(\mathbf{k}'). \quad (\text{S24})$$

The largest eigenvalue λ_α of equation (S24) results in the highest transition temperature [18], while λ_α in general determines the pairing strength for the different pairing channels α [21]. The corresponding gap symmetries are identified by the eigenfunction $f_\alpha(\mathbf{k})$. The inverse of the Fermi velocity $v_F(\mathbf{k}) = |\nabla_{\mathbf{k}} E_\nu(\mathbf{k})|$ gives a measure of the DOS and momenta $\mathbf{k} \in C_i$, $\mathbf{k}' \in C_j$ are constrained to the FS sheets $C_{i,j}$. In Eq. (S24), $\tilde{\Gamma}_{ij}(\mathbf{k}, \mathbf{k}')$ represents the renormalized form of the effective multiorbital pair scattering vertex and is given by

$$\tilde{\Gamma}_{ij}(\mathbf{k}, \mathbf{k}') = \text{Re} \sum_{l_1 l_2 l_3 l_4} \sqrt{Z_{l_1}} \sqrt{Z_{l_4}} a_{\nu_i}^{l_1,*}(\mathbf{k}) a_{\nu_j}^{l_4,*}(-\mathbf{k}) \tilde{\Gamma}_{l_1 l_2 l_3 l_4}^{S/T}(\mathbf{k}, \mathbf{k}', \omega = 0) \sqrt{Z_{l_2}} \sqrt{Z_{l_3}} a_{\nu_j}^{l_2}(\mathbf{k}') a_{\nu_i}^{l_3}(-\mathbf{k}'), \quad (\text{S25})$$

$$\tilde{\Gamma}_{l_1 l_2 l_3 l_4}^S(\mathbf{k}, \mathbf{k}', \omega) = \left[\frac{3}{2} U^s \tilde{\chi}_{l_1 l_2 l_3 l_4}^{\text{RPA}, s}(\mathbf{k} - \mathbf{k}') U^s + \frac{1}{2} U^s - \frac{1}{2} U^c \tilde{\chi}_{l_1 l_2 l_3 l_4}^{\text{RPA}, c}(\mathbf{k} - \mathbf{k}') U^c + \frac{1}{2} U^c \right]_{l_1 l_2 l_3 l_4}, \quad (\text{S26})$$

$$\tilde{\Gamma}_{l_1 l_2 l_3 l_4}^T(\mathbf{k}, \mathbf{k}', \omega) = \left[-\frac{1}{2} U^s \tilde{\chi}_{l_1 l_2 l_3 l_4}^{\text{RPA}, s}(\mathbf{k} - \mathbf{k}') U^s + \frac{1}{2} U^s - \frac{1}{2} U^c \tilde{\chi}_{l_1 l_2 l_3 l_4}^{\text{RPA}, c}(\mathbf{k} - \mathbf{k}') U^c + \frac{1}{2} U^c \right]_{l_1 l_2 l_3 l_4}. \quad (\text{S27})$$

Here, $\tilde{\Gamma}_{l_1 l_2 l_3 l_4}$ determines the orbital vertex functions in the singlet (S) and triplet (T) channel. Physically, $\tilde{\Gamma}_{l_1 l_2 l_3 l_4}$ reflects particle-particle scattering of electrons from orbitals l_1, l_4 into orbitals l_2, l_3 . The quantities $U^s, U^c, \chi^{\text{RPA}}$ are matrices in orbital space and $\chi^{\text{RPA}, s/c}$ describes spin or charge fluctuations, respectively.

IV. STABILITY OF RPA ANALYSIS WITH RESPECT TO TB PARAMETERS

A recent debate regarding the pairing symmetry in the $\text{La}_3\text{Ni}_2\text{O}_7$ nickelate system [22, 23] stresses the importance of potential sensitivity of the RPA method to details of the input band structure and interaction parameters. In order to ensure the robustness of our results not just with respect to quasiparticle renormalization and interaction strength, which we discuss in the main text, we also investigate the impact of small modification to the TB model. When doing so, our aim is to keep the overall FS topology close to the one of the unchanged TB model. This results in a limitation of the variation of the hopping amplitudes. If, for instance, we vary the parameter t_{11}^z by $\pm 5\%$, the pocket around Γ notably changes in size, as can be seen in Fig. S4. For larger changes, it would eventually vanish or touch the Ni $3d_{x^2-y^2}$ dominated surface, which represents a major deviation from the original fermiology. We take this as a point of reference and calculate the pairing symmetries for $\pm 5\%$ changes to the largest hopping amplitudes, i.e., $t_{11}^x, t_{11}^z, t_{22}^x, t_{22}^z$, and t_{33}^x .

As a result, we find that in all cases the leading solution still remains a degenerate (p_x, p_y) -wave state. In Table I, we list the corresponding ratio λ_T/λ_S of leading triplet over singlet eigenvalue for $U_{\text{La}}/U_{\text{Ni}} = 0.5$, $J_{\text{La}}/U_{\text{La}} = 0.2$, $U_{\text{Ni}} = 5 \text{ eV}$ and 20 eV , as well as $Z_{d_{x^2-y^2}} = 0.15$. Another modification that leaves the general FS topology intact would be given by alteration of the interorbital, i.e., hybridization terms in the Hamiltonian. Here, we checked the extreme case of essentially neglecting hybridization by setting all t_{12}, t_{13} , or t_{23} amplitudes to zero, both individually or together. Exemplary calculations with $J_{\text{La}}/U_{\text{La}} = 0.2$ and $U_{\text{Ni}} = 5 \text{ eV}$ show negligible changes of λ_T/λ_S , while confirming the degenerate p -wave solution. Hence, we conclude that our DFT band structure indeed permits a reliable RPA analysis and physically reasonable modifications to the TB model do not significantly alter the leading terms of the pairing symmetries.

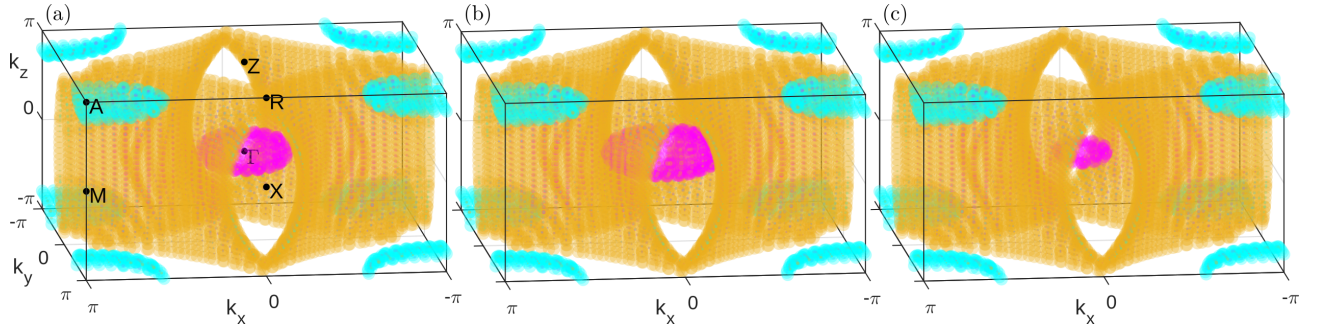


FIG. S4. 3D Fermi surfaces, with magenta, cyan, and yellow color referring to La d_{z^2} , La d_{xy} , and Ni $d_{x^2-y^2}$ orbital contributions, respectively. Shown are (a) the FS from the unchanged TB model, (b) the results from increasing t_{11}^z by 5%, and (c) from reducing t_{11}^z by 5%.

U_{Ni}	unchanged	$0.95 t_{11}^x$	$1.05 t_{11}^x$	$0.95 t_{11}^z$	$1.05 t_{11}^z$	$0.95 t_{22}^x$	$1.05 t_{22}^x$	$0.95 t_{22}^z$	$1.05 t_{22}^z$	$0.95 t_{33}^x$	$1.05 t_{33}^x$
5	3.67	3.16	3.73	2.95	3.69	3.47	3.30	3.90	3.44	3.71	3.56
20	2.53	1.85	3.96	1.75	4.81	2.48	2.41	2.55	2.47	2.48	2.50

TABLE I. Ratio λ_T/λ_S of the eigenvalues of the favored triplet and singlet channel for $U_{\text{La}}/U_{\text{Ni}} = 0.5$, $J_{\text{La}}/U_{\text{La}} = 0.2$, and $Z_{d_{x^2-y^2}} = 0.15$. The pairing symmetry remains E_u throughout.

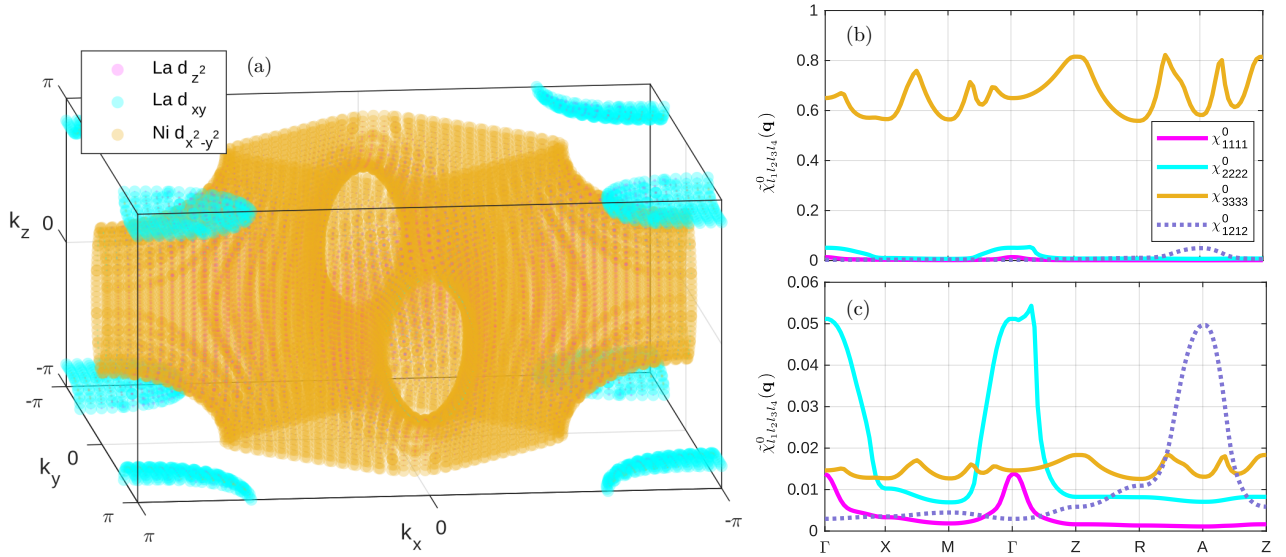


FIG. S5. (a) 3D Fermi surface including the orbital contributions relevant for the low-energy description of doped LaNiO₂. Magenta, cyan, and yellow refer to the La d_{z^2} , La d_{xy} , and Ni $d_{x^2-y^2}$ orbitals, respectively. (b), (c) Static bare susceptibilities $\tilde{\chi}_{l_1 l_2 l_3 l_4}^0(\mathbf{q}, \omega = 0)$ for (b) $Z_{d_{x^2-y^2}} = 1$ and (c) $Z_{d_{x^2-y^2}} = 0.15$ for doped LaNiO₂. The interorbital susceptibility $\tilde{\chi}_{1212}^0$ is shown in purple. The mesh for momentum space integration includes $80 \times 80 \times 80$ \mathbf{k} -points.

V. DOPED LaNiO₂

Another natural question is whether the observed odd-parity p -wave state is also realized in doped LaNiO₂. To investigate this, we capture the essential impact of doping by a rigid shift of the chemical potential, such that the Γ -centered electron pocket is lifted above the Fermi level. We show the corresponding 3D FS in Fig. S5(a). In the next step, we analyze the bare susceptibilities shown in Figs. S5(b) and S5(c). On the one hand, the diagonal susceptibility $\tilde{\chi}_{3333}^0$ loses its main peaks around the A and M points. On the other hand, once we introduce correlations by setting $Z_{d_{x^2-y^2}} = 0.15$, the central features are again given by the intraorbital rare-earth contributions $\tilde{\chi}_{1111}^0$ and $\tilde{\chi}_{2222}^0$ around Γ , as well as the interorbital component $\tilde{\chi}_{1212}^0$ around A. In contrast to undoped LaNiO₂, the intraorbital La d_{xy} susceptibility $\tilde{\chi}_{2222}^0$ now far surpasses $\tilde{\chi}_{1111}^0$ from the La d_{z^2} orbital. This is not surprising since La d_{z^2} electrons used to contribute mainly to the pocket around Γ , which has vanished due to doping.

Finally, we also perform calculations of the pairing symmetry in doped LaNiO₂, which can be seen in Fig. S6. Most interestingly, we observe that the essential conclusions made for the SC state of the undoped compound are still valid. The gap now

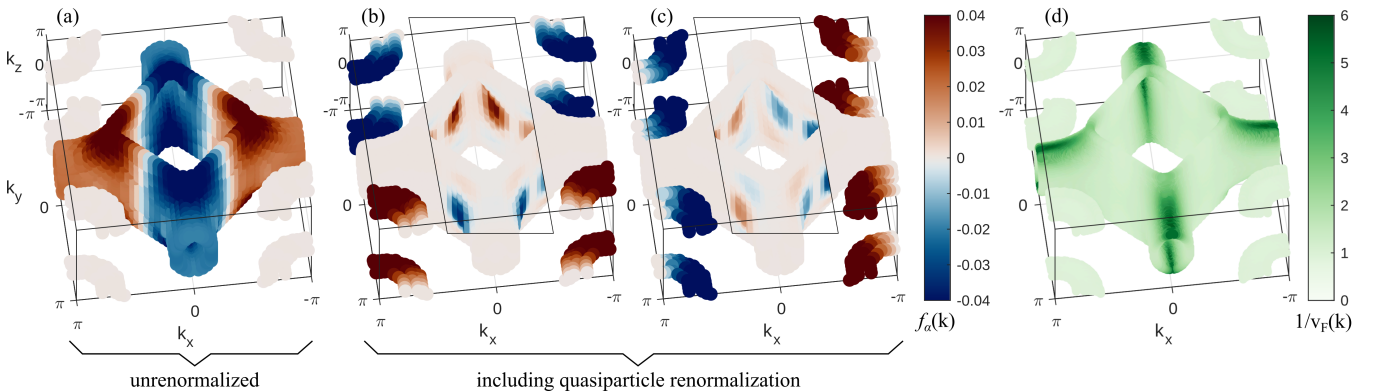


FIG. S6. Leading pairing structure of doped LaNiO₂ with and without inclusion of quasiparticle renormalization for (a) $Z_{d_{x^2-y^2}} = 1$ and (b), (c) $Z_{d_{x^2-y^2}} = 0.15$. The gap symmetry transitions from (a) an even-parity d -wave to (b), (c) a degenerate odd-parity p -wave solution. A color scale highlighting smaller amplitudes with maximum value of $\pm 1 \times 10^{-4}$ was chosen for the insets to reveal the sign change on the large FS as a function of k_z . In (d) the momentum-dependent inverse Fermi-velocity $1/v_F(\mathbf{k}) = 1/|\nabla_{\mathbf{k}} E_F(\mathbf{k})|$ gives a measure of the DOS. A total of 6800 points is taken for the 3D gap-structure calculations and we use $60 \times 60 \times 60$ \mathbf{k} -points for momentum space integration.

clearly dominates on the remaining rare-earth pockets around A. In fact, the transition to a favored p -wave happens for even bigger quasiparticle weights of $Z_{d_{x^2-y^2}} \lesssim 0.3$, which might be facilitated due to a reduced DOS at the van Hove features around R. For $Z_{d_{x^2-y^2}} = 0.15$, $U_{\text{La}}/U_{\text{Ni}} = 0.5$, $J_{\text{La}}/U_{\text{La}} = 0.2$ and $U_{\text{Ni}} = 5$ eV, the eigenvalue λ_T of the degenerate leading triplet solutions, i.e., their pairing strength, reaches $\lambda_T \approx 8.99\lambda_S$, with λ_S belonging to the leading singlet state. Intriguingly, this ratio is even greater than in pristine LaNiO_2 , where $\lambda_T \approx 3.67\lambda_S$ for the same set of parameters. However, note that doping reduces the effective-mass enhancement and thus could have a compensating effect.

-
- [1] G. Kresse and D. Joubert, From ultrasoft pseudopotentials to the projector augmented-wave method, *Phys. Rev. B* **59**, 1758 (1999).
 - [2] G. Kresse and J. Furthmüller, Efficient iterative schemes for ab initio total-energy calculations using a plane-wave basis set, *Phys. Rev. B* **54**, 11169 (1996).
 - [3] P. E. Blöchl, Projector augmented-wave method, *Phys. Rev. B* **50**, 17953 (1994).
 - [4] J. P. Perdew, J. A. Chevary, S. H. Vosko, K. A. Jackson, M. R. Pederson, D. J. Singh, and C. Fiolhais, Atoms, molecules, solids, and surfaces: Applications of the generalized gradient approximation for exchange and correlation, *Phys. Rev. B* **46**, 6671 (1992).
 - [5] A. D. Becke, Density-functional exchange-energy approximation with correct asymptotic behavior, *Phys. Rev. A* **38**, 3098 (1988).
 - [6] D. C. Langreth and M. J. Mehl, Beyond the local-density approximation in calculations of ground-state electronic properties, *Phys. Rev. B* **28**, 1809 (1983).
 - [7] J. P. Perdew, K. Burke, and M. Ernzerhof, Generalized gradient approximation made simple, *Phys. Rev. Lett.* **77**, 3865 (1996).
 - [8] G. H. Wannier, The structure of electronic excitation levels in insulating crystals, *Phys. Rev.* **52**, 191 (1937).
 - [9] G. H. Wannier, Dynamics of band electrons in electric and magnetic fields, *Rev. Mod. Phys.* **34**, 645 (1962).
 - [10] A. A. Mostofi, J. R. Yates, G. Pizzi, Y.-S. Lee, I. Souza, D. Vanderbilt, and N. Marzari, An updated version of wannier90: A tool for obtaining maximally-localised wannier functions, *Comp. Phys. Commun.* **185**, 2309 (2014).
 - [11] N. Marzari, A. A. Mostofi, J. R. Yates, I. Souza, and D. Vanderbilt, Maximally localized wannier functions: Theory and applications, *Rev. Mod. Phys.* **84**, 1419 (2012).
 - [12] N. Marzari and D. Vanderbilt, Maximally localized generalized wannier functions for composite energy bands, *Phys. Rev. B* **56**, 12847 (1997).
 - [13] I. Souza, N. Marzari, and D. Vanderbilt, Maximally localized wannier functions for entangled energy bands, *Phys. Rev. B* **65**, 035109 (2001).
 - [14] V. Wang, N. Xu, J.-C. Liu, G. Tang, and W.-T. Geng, Vaspkit: A user-friendly interface facilitating high-throughput computing and analysis using vasp code, *Comp. Phys. Commun.* **267**, 108033 (2021).
 - [15] K. Momma and F. Izumi, *VESTA*: a three-dimensional visualization system for electronic and structural analysis, *Journ. Appl. Cryst.* **41**, 653 (2008).
 - [16] Y. Yamakawa, S. Onari, and H. Kontani, Nematicity and Magnetism in FeSe and Other Families of Fe-Based Superconductors, *Phys. Rev. X* **6**, 021032 (2016).
 - [17] A. Kreisel, B. M. Andersen, P. O. Sprau, A. Kostin, J. C. S. Davis, and P. J. Hirschfeld, Orbital selective pairing and gap structures of iron-based superconductors, *Phys. Rev. B* **95**, 174504 (2017).
 - [18] S. Graser, T. A. Maier, P. J. Hirschfeld, and D. J. Scalapino, Near-degeneracy of several pairing channels in multiorbital models for the Fe pnictides, *New J. Phys.* **11**, 025016 (2009).
 - [19] A. T. Rømer, A. Kreisel, I. Eremin, M. A. Malakhov, T. A. Maier, P. J. Hirschfeld, and B. M. Andersen, Pairing symmetry of the one-band hubbard model in the paramagnetic weak-coupling limit: A numerical RPA study, *Phys. Rev. B* **92**, 104505 (2015).
 - [20] A. F. Kemper, T. A. Maier, S. Graser, H.-P. Cheng, P. J. Hirschfeld, and D. J. Scalapino, Sensitivity of the superconducting state and magnetic susceptibility to key aspects of electronic structure in ferropnictides, *New J. Phys.* **12**, 073030 (2010).
 - [21] D. J. Scalapino, E. Loh, and J. E. Hirsch, d -wave pairing near a spin-density-wave instability, *Phys. Rev. B* **34**, 8190 (1986).
 - [22] Y.-B. Liu, J.-W. Mei, F. Ye, W.-Q. Chen, and F. Yang, s_{\pm} -Wave Pairing and the Destructive Role of Apical-Oxygen Deficiencies in $\text{La}_3\text{Ni}_2\text{O}_7$ under Pressure, *Phys. Rev. Lett.* **131**, 236002 (2023).
 - [23] G. Heier, K. Park, and S. Y. Savrasov, Competing d_{xy} and s_{\pm} pairing symmetries in superconducting $\text{La}_3\text{Ni}_2\text{O}_7$: LDA + FLEX calculations, *Phys. Rev. B* **109**, 104508 (2024).